



Combined infrared and ab initio study of the $\text{H}_2\text{-HN}_2^+$ complex[☆]

E.J. Bieske*, S.A. Nizkorodov, F.R. Bennett, J.P. Maier

Institute für Physikalische Chemie, Universität Basel, Klingelbergstr. 80, Basel, CH-4056, Switzerland

Received 24 March 1995; accepted 31 May 1995

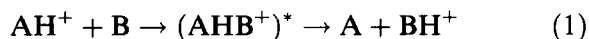
Abstract

Combined spectroscopic and ab initio studies of the $\text{H}_2\text{-HN}_2^+$ proton-bound complex are presented. Infrared spectra of mass-selected $\text{H}_2\text{-HN}_2^+$ complexes in the $2500\text{--}4200\text{ cm}^{-1}$ range display a number of vibrational bands, assigned as due either to the H–H stretch vibration, or tentatively to the N–H stretch in combination with *intermolecular* stretch and bend motions. Due to subpicosecond energy redistribution, almost all rotational structure is obscured by lifetime broadening. The ab initio calculations conducted at the QCISD(T)/6-311G(2df,2pd) level indicate that the complex is composed of largely undistorted H_2 and HN_2^+ subunits, and has a T-shaped minimum energy geometry with an $\text{H}_2\cdots\text{HN}_2^+$ intermolecular bond length of approximately 1.44 \AA . Both spectral and theoretical results show that combining the H_2 and HN_2^+ molecules drastically reduces the frequency of the N–H stretch vibration, although the H_2 stretch frequency is only modestly affected.

Keywords: Ab initio studies; $\text{H}_2\text{-HN}_2^+$ complex; Infrared spectra

1. Introduction

The fundamental chemical role of gas phase proton transfer reactions



in both terrestrial and astrophysical plasmas has, over the years, motivated considerable experimental and theoretical effort. On the experimental side, the need for accurate reaction rate constants for reactions such as (1) has provided impetus for the development of sophisticated experimental apparatus in

which ion/molecule reactions can be characterized at specific temperatures without the distraction of interfering reactions. One of the most successful approaches in this regard has been the selected-ion flow tube (SIFT) technique developed in the mid 1970s by Adams and Smith [1,2]. Measurements of the rate constant for reaction (1) using SIFT (and other techniques) suggest that in most cases when the transfer is exothermic, it occurs without activation barrier, proceeding with a rate consistent with the action of long-range electrostatic and inductive attractions.

Despite our insight into the of factors governing the rate of reaction (1) there remain many features that are poorly understood. These largely relate to microscopic aspects of

[☆] Dedicated to Professor David Smith on the occasion of his 60th birthday.

* Corresponding author.

the reaction, and include such matters as product energy distributions (translational, rotational, vibrational) and branching ratios between various product isomers. From a theoretical viewpoint, explanation of such features requires a more comprehensive understanding of the entire reaction potential energy surface (PES). One experimental approach to the exploration and characterization of proton transfer PESs involves creating and spectroscopically characterizing small proton-bound complexes, species that can be viewed as de-energized reaction intermediates. Through observation of vibrational bands associated with intermolecular and intramolecular vibrational motion, and in some cases through resolution of rotational structure, one can derive direct impressions of the PES in regions adjacent to the minimum. In the current work we detail our studies of $\text{H}_2\text{-HN}_2^+$, a complex that may be viewed as a stabilized intermediate for the exothermic $\text{H}_3^+ + \text{N}_2 \rightarrow \text{HN}_2^+ + \text{H}_2$ ($\Delta H \approx -18 \text{ kcal mol}^{-1}$) [3] proton transfer reaction. Although the current work is the first to address structural aspects of $\text{H}_2\text{-HN}_2^+$ by examining its infrared absorptions, there have been previous experimental and theoretical studies. Particularly significant are thermochemical high pressure mass spectrometry data which demonstrate that the complex is reasonably strongly bound, having a heat of formation from $\text{HN}_2^+ + \text{H}_2$ of $7.2 \text{ kcal mol}^{-1}$ [4] ($\approx 2520 \text{ cm}^{-1}$). Thus the energy range of our spectroscopic investigations ($2500\text{--}4200 \text{ cm}^{-1}$) begins close to the dissociation threshold.

The $\text{H}_2\text{-HN}_2^+$ complex is one of an increasing number of proton-bound species, including $\text{H}_3^+(\text{H}_2)_n$ [5], $\text{H}_2\text{-H}_3\text{O}^+$ [6], $\text{H}_3\text{O}^+(\text{H}_2\text{O})_n$ [6], $\text{NH}_4^+(\text{NH}_3)_n$ [7], $\text{H}_2\text{-HCO}^+$ [8] and He-HN_2^+ [9], which have been subjected to spectroscopic scrutiny in the mid-infrared part of the spectrum. Generally the spectra have been obtained by monitoring the appearance of photofragment ions after exciting the

complexes to a predissociative vibrational level. Unfortunately the spectra obtained in this manner are often lifetime broadened due to rapid upper state energy redistribution, frustrating to some extent efforts to extract precise structural information. However, even in these cases, structures have been convincingly inferred from the disposition and strength of vibrational bands, often with some guidance from accompanying ab initio calculations, and evidence from high pressure mass spectrometry measurements (providing clustering enthalpies and entropies). In some favourable systems ($\text{H}_2\text{-HCO}^+$ [8] and He-HN_2^+ [9]) full rotational resolution has been achieved, allowing determination of accurate spectroscopic constants. Unfortunately this is not the case for $\text{H}_2\text{-HN}_2^+$ and structural inferences reached in this paper are based on ab initio calculations and analysis of experimental vibrational band shifts and band shapes. Nonetheless, taken together with an earlier study of the $\text{H}_2\text{-HCO}^+$ complex, the current work provides direct insights into factors governing the structural and dynamical properties of proton-bound complexes.

2. Experimental

The experiment involves infrared excitation of predissociative vibrational levels of $\text{H}_2\text{-HN}_2^+$ complexes in a tandem mass spectrometer. As detailed descriptions of the apparatus are available in the literature [10–12] only a cursory overview is provided here. In brief, ions from the cluster ion source are injected into a quadrupole mass filter where mass selection of the primary ion beam is accomplished. The resulting beam is deflected through 90° by an electrostatic quadrupole bender and injected into an octopole ion guide. Here the ions are subjected to the counter-propagating output of a pulsed tunable optical parametric oscillator (OPO).

Any HN_2^+ fragments produced through the action of the light, or from either metastable or collision-induced decay, are transmitted by a second quadrupole mass filter, with the current being measured by a Daly scintillation detector in combination with a boxcar integrator. The machine is operated in a pulsed mode (40 Hz) with the laser fired at half the frequency, so that the metastable and collision-induced contributions can be accounted for by subtracting the laser-off signal from laser-on signals.

The ion source consists of pulsed supersonic expansion with twin electron-emitting filaments positioned slightly downstream of the nozzle orifice. In the present experiment a 15:1 mixture of H_2 and N_2 was passed through a liquid nitrogen cooled trap to remove water vapour and expanded at 4–5 atm. An on-line computer-controlled gas-mixing system provides flexibility in optimizing the gas mixture. Adjustment of source conditions to produce $\text{H}_2\text{-HN}_2^+$ was achieved initially by introducing Ar or He buffer gas into the octopole region and monitoring the collision-induced fragmentation into HN_2^+ . Subsequently, the photofragmentation signal was maximized with the laser tuned to a resonance. Previous studies have shown that the source is capable of producing ionic complexes with rotational temperatures in the 30–40 K range, although on occasion the vibrational temperature can be considerably higher.

Infrared photons for the dissociation of the complex were generated in an OPO consisting of an oscillator stage, a second stage which produces near-infrared radiation and a final stage issuing narrow band radiation in the 2500–4000 cm^{-1} range with a bandwidth of 0.02 cm^{-1} . Wavelength calibration was achieved by directing some fraction of the light into a reference optoacoustic cell filled with either H_2O or C_2H_2 . Further details of this part of the spectrometer can be found in Ref. [8].

3. Ab initio calculations

In this section the ab initio computations of the $\text{H}_2\text{-HN}_2^+$ complex are described. Before presenting the results, it is useful to outline structural characteristics expected on the basis of electrostatic considerations. For a more comprehensive discussion of the iso-electronic $\text{H}_2\text{-HCO}^+$ molecule the reader may care to consult Ref. [8]. Due to the somewhat higher proton affinity of N_2 one expects that the complex will essentially consist of an H_2 ligand bound to the linear HN_2^+ molecule. Classically, at long range, stabilization of the complex should arise from the $1/R^3$ charge–quadrupole electrostatic interaction between H_2 and HN_2^+ molecules supplemented by a $1/R^4$ inductive charge-induced dipole contribution, i.e.

$$V_{\text{lr}}(R, \theta) = \frac{Q\Theta}{8\pi\epsilon_0 R^3} \times (3 \cos^2 \theta - 1) - \frac{1}{2} \frac{Q^2(\alpha_{\parallel} \cos^2 \theta + \alpha_{\perp} \sin^2 \theta)}{4\pi\epsilon_0 R^4} \quad (2)$$

(where Q is the ion charge, R the distance between the H_2 centre of mass and the ion, α_{\parallel} and α_{\perp} the parallel and perpendicular volume polarizabilities of H_2 (0.93 \AA^3 and 0.79 \AA^3 respectively [13]), and Θ the quadrupole moment of H_2 ($+2.12 \times 10^{-40} \text{ C m}^2$ [14]). While the induction force is attractive for any orientation of the H_2 with respect to the HN_2^+ , the charge–quadrupole force is repulsive in the linear configuration and strongly favours a T-shaped structure (the predicted barrier for internal rotation of the H_2 at a distance of 2.5 \AA from a charge is approximately 1150 cm^{-1}).

The structural expectations outlined in the previous paragraph are supported by previous ab initio calculations [15] which show that when constrained to a T-shaped configuration the H_2 is relatively strongly bound to the protonated end of HN_2^+ ($D_e = 6.8 \text{ kcal mol}^{-1}$,

$R_{\text{int}} = 1.53 \text{ \AA}$) with minimal distortion of the monomer subunits. The same calculations indicate that attachment of the H_2 to the nitrogen end results in a substantially weaker bond ($D_e = 0.7 \text{ kcal mol}^{-1}$) and longer intermolecular separation ($R_{\text{int}} = 2.10 \text{ \AA}$ [15]).

In the earlier study on the analogous $\text{H}_2\text{-HCO}^+$ complex [8] we found that ab initio molecular orbital calculations were able to provide structural and spectroscopic information to satisfactory accuracy. We therefore decided to treat $\text{H}_2\text{-HN}_2^+$ with a similar theoretical approach. Quadratic configuration interaction (QCI) calculations [16] were performed to determine theoretical values for the equilibrium structure, dissociation energy and harmonic vibrational frequencies for the ion/molecule complex. The QCI calculations employed standard QCISD(T) wavefunctions whereby all single and double excitations from a single closed-shell Hartree–Fock (HF) determinant, within the frozen core approximation, construct the CI space (QCISD). Once convergence of the QCISD wavefunction is achieved, a final non-iterative step approximates the perturbative effect of triple excitations on the QCISD wavefunction to give the final QCISD (T) wavefunction. This variant of coupled cluster theory has been shown in several studies to give very accurate results where suitably large basis sets are used and the HF determinants forms the dominant part of the CI vector.

Two gaussian basis sets have been used in this study, providing a compromise between accuracy and expense. Equilibrium geometries and reaction energies were determined using the 6-311G(2df,2pd) basis set of Krishnan et al. [17]. Pruning this basis set by removing the two outermost polarization functions on each atom (i.e. one p and d function from hydrogen and one d and f function from nitrogen) gives the 6-311G(d,p) basis which was used to construct a quadratic force field for the calculation of harmonic frequencies. All

calculations were performed using the GAUSSIAN 92 program suite [18].

The calculated equilibrium structures of the separate monomers, H_2 and HN_2^+ , were in close agreement with the experimentally determined geometries, with $r(\text{N-H}) = 1.033 \text{ \AA}$ and $r(\text{N-N}) = 1.099 \text{ \AA}$ in HN_2^+ compared to the experimental values of $r(\text{NH}) = 1.032 \text{ \AA}$ and $r(\text{N-N}) = 1.094 \text{ \AA}$ [19]. Satisfactory concurrence between calculated ($\nu_1 = 3426 \text{ cm}^{-1}$, $\nu_2 = 700 \text{ cm}^{-1}$, $\nu_3 = 2264 \text{ cm}^{-1}$) and experimental ($\nu_1 = 3234 \text{ cm}^{-1}$, $\nu_2 = 688 \text{ cm}^{-1}$, $\nu_3 = 2258 \text{ cm}^{-1}$) [20] vibrational frequencies is also found. The calculated frequencies are typically overestimated due to the neglect of anharmonic contributions, and a more direct comparison may be made with the experimental harmonic frequencies ($\nu_1 = 3405 \text{ cm}^{-1}$, $\nu_2 = 693 \text{ cm}^{-1}$, $\nu_3 = 2266 \text{ cm}^{-1}$) [20]. A similar situation is found when the calculated H_2 stretching frequency of 4402 cm^{-1} is compared to the experimental first vibrational spacing of 4161 cm^{-1} [21], the discrepancy once again being largely attributable to anharmonicity in the H_2 potential.

The $\text{H}_2\text{-HN}_2^+$ complex prefers a C_{2v} structure consisting of largely undistorted H_2 and HN_2^+ subunits as shown in Fig. 1. The calculated intermolecular bond length of 1.435 \AA is significantly shorter than previous theoretical predictions of 1.657 \AA [22] and 1.53 \AA [15] employing limited basis sets and CISD wavefunctions, with the difference perhaps due to basis set incompleteness in the earlier studies. For example, in preparatory calculations carried out on the $\text{H}_2\text{-HN}_2^+$ complex at the QCISD level, we noticed a contraction in the intermolecular bond length of some 0.07 \AA in going from a 6-31G(d,p) to a 6-311G(2df,2pd) basis set. The D_0 for the intermolecular bond energy is calculated to be $5.71 \text{ kcal mol}^{-1}$ including zero-point, harmonic vibrational energy corrections. The zero-point energies were determined from the calculated harmonic frequencies which were scaled by 0.95 to

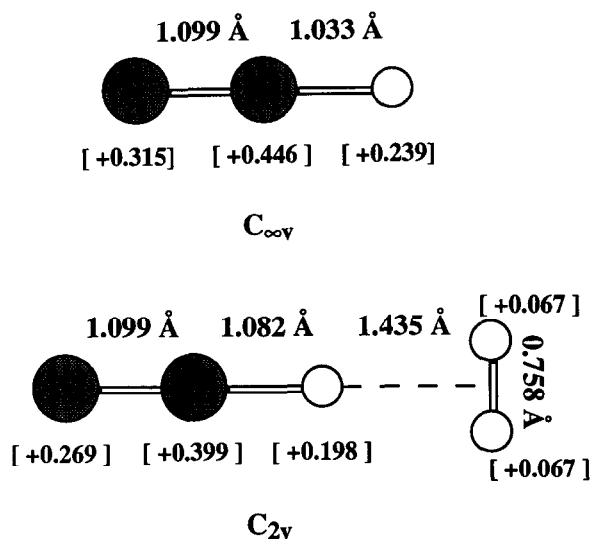


Fig. 1. Minimum energy structure for $\text{H}_2\text{-HN}_2^+$ and HN_2^+ calculated at the QCISD(T)/6-311G(2df,2pd) level. The complex consists of essentially undistorted H_2 and HN_2^+ subunits bound together in a T-shaped fashion. The numbers shown in parentheses are Mulliken atomic charges calculated on the basis of the QCISD/6-311G(2df,2pd)//QCISD(T)/6-311G(2df,2pd) density matrix.

account in an approximate way for anharmonic contributions (see Ref. [23] for discussions). Although an experimental value for D_0 has not been reported, thermochemical experiments provide an enthalpy for the $\text{H}_2 + \text{HN}_2^+ \rightarrow \text{H}_2\text{-HN}_2^+$ association reaction of $\Delta H^0 = -7.2 \pm 0.2 \text{ kcal mol}^{-1}$ [4]. Once the necessary thermodynamical corrections are made to the calculated bond energy [24] a theoretical value of $\Delta H^0 = -6.5 \text{ kcal mol}^{-1}$ is extracted, providing satisfactory agreement with the experimental value.

The normal vibrational modes of $\text{H}_2\text{-HN}_2^+$ (Fig. 2) can be factored into two categories: low frequency vibrations associated with intermolecular motions and higher frequency intramolecular modes connected with deformation of the molecular subunits. Vibrations in the latter category should be similar in nature to those of the isolated monomeric subunits. For example, the ν_1 vibration of $\text{H}_2\text{-HN}_2^+$ can be compared to the H_2 stretch, ν_2 and ν_3 respectively with the N–H and N–N stretches of

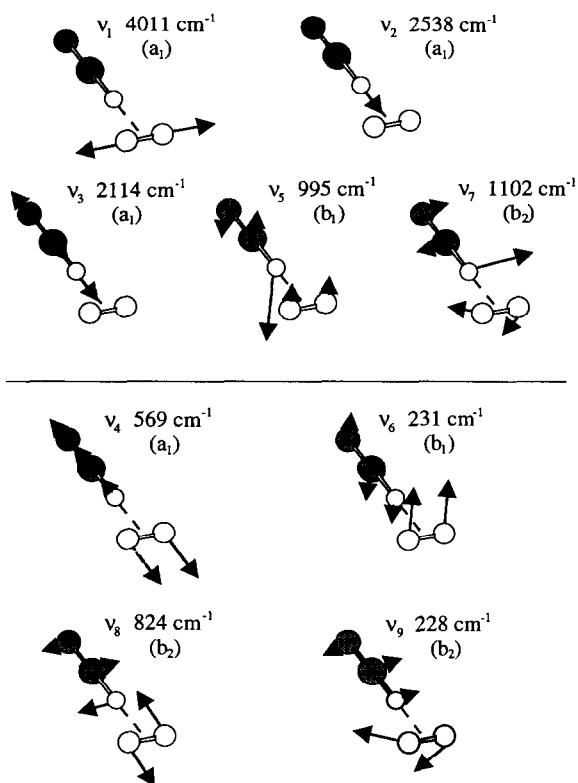


Fig. 2. Schematic representation of $\text{H}_2\text{-HN}_2^+$ vibrational motions. Vibrations confined principally to the monomer constituents (intramolecular vibrations) are shown in the upper part of the figure, while the vibrations involving relative motions of the components (intermolecular motions) are displayed at the bottom.

HN_2^+ , and ν_5 and ν_7 with the degenerate bend of HN_2^+ . It should be reasonable to assume that the anharmonicity of the intramolecular vibrations is not greatly altered when the constituents are brought together to form the complex, so that a fair guide to the complexes' intramolecular frequencies should be attained by scaling each frequency by the factor necessary to bring the corresponding calculated monomer frequencies into line with the experimental ones. These scaled frequencies are given in Fig. 2 and are also provided in Table 1 along with the unscaled anharmonic frequencies.

The effects of anharmonicity are likely to be greater for intermolecular modes than they are

Table 1
Ab initio harmonic vibrational frequencies and band transition moments predicted at the QCISD(T) 6-311G(d,p) level of theory.

Mode	Symmetry	Description	Frequency (cm ⁻¹)	Dipole strength (D ²)
1	a ₁	H–H stretch	4243 (4011)	5.2 × 10 ⁻³
2	a ₁	N–H stretch	2689 (2538)	2.7 × 10 ⁻¹
3	a ₁	N–N stretch	2122 (2114)	1.6 × 10 ⁻¹
4	a ₁	Intermolecular stretch	569	1.1 × 10 ⁻¹
5	b ₁	HNN out-of-plane bend	1014 (995)	3.3 × 10 ⁻²
6	b ₁	Low frequency out-of-plane bend	231	5.8 × 10 ⁻⁶
7	b ₂	HNN in-plane bend	1123 (1101)	8.0 × 10 ⁻³
8	b ₂	H ₂ rock	824	3.1 × 10 ⁻²
9	b ₂	Low frequency in-plane bend	228	1.5 × 10 ⁻⁴

Intramolecular frequencies which have been scaled by a factor necessary to bring the corresponding calculated H₂ and HN₂⁺ monomer frequencies into line with the experimental ones are given in brackets (see text).

for the intramolecular ones, perhaps rendering the calculated vibrational frequencies somewhat unreliable. It is possible, however, to investigate the anharmonic nature of the intermolecular stretch by generating an effective stretching potential, whereby electronic energy calculations are performed at a number of different fixed intermolecular separations, whilst allowing the remaining internal coordinates to relax energetically. Equipped with the resulting potential, shown in Fig. 3, the radial Schrödinger equation was solved numerically to yield vibrational energy levels [25]. As expected, due to the anharmonicity of the potential energy function the first vibrational energy spacing calculated from the effective potential (438 cm⁻¹) is somewhat lower than the corresponding harmonic frequency (569 cm⁻¹).

A qualitative impression of the nature of the HN₂⁺ ··· H₂ intermolecular bond can be developed by inspecting the Mulliken populations on each atomic centre. For this purpose, calculations were carried out at the QCISD

/6-311G(2df,2pd)//QCISD(T)/6-311G(2df,2pd) level to construct a one-particle density matrix based upon a highly correlated wavefunction. The resulting Mulliken analysis indicates a migration of 0.134 e of electron density away from the H₂ moiety (see Fig. 1). It is interesting to note that according to the Mulliken analysis, the electron density gained by the HN₂⁺

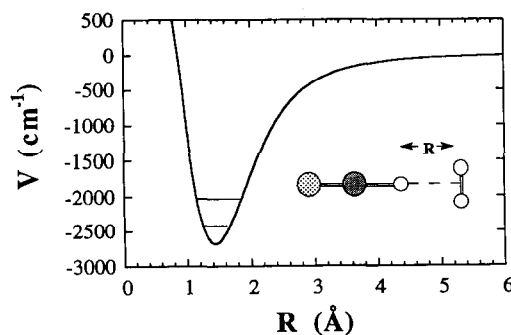


Fig. 3. Intermolecular stretching potential for H₂ ··· HN₂⁺, determined by varying the H₂ ··· HN₂⁺ intermolecular separation whilst allowing all other degrees of freedom to relax. Vibrational level spacings were determined by numerically solving the radial Schrödinger equation [25].

subunit upon association with H_2 is roughly equally shared by all HN_2^+ atomic constituents.

4. Results and assignments

The vibrational predissociation spectrum of $\text{H}_2\text{-HN}_2^+$ has been recorded in a series of shorter scans (each approximately 100–200 cm^{-1} long) which have been pieced together to produce the spectrum displayed in Fig. 4 (band positions given in Table 2). Although relative intensities of adjacent vibrational bands should be more or less correct, this will be less true for bands separated by large energy gaps. While none of the prominent vibrational bands occurring in the 2500–4200 cm^{-1} range displays well-resolved rotational lines, there do appear to be two distinct types of rotational band contours, corresponding to infrared transitions in a near-prolate symmetric top with the transition moment either parallel or perpendicular to the A axis. The 3962 cm^{-1} band (shown in more detail in Fig. 5) is an example of a parallel transition, and exhibits a pronounced

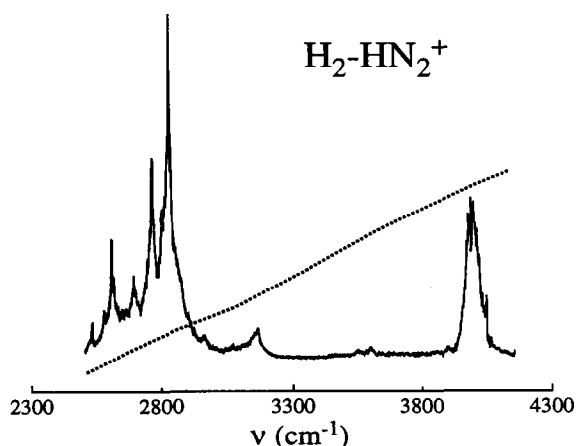


Fig. 4. Vibrational predissociation spectrum of $\text{H}_2\text{-HN}_2^+$ in the 2500–4200 cm^{-1} range recorded by monitoring the HN_2^+ photoyield. The relative intensities of different bands may be somewhat distorted, as the spectrum is a composite built up from several shorter scans, and is not corrected for laser power (shown as the dotted curve).

Table 2

Experimental vibrational band positions and estimated intensities for the $\text{H}_2\text{-HN}_2^+$ complex in the 2500–4200 cm^{-1} range.

Position (cm^{-1})	Estimated intensity	Assignment
2534	Weak	
2580	Weak	
2609	Medium	
2618	Weak	
2693	Medium	
2766	Strong	
2803	Medium	
2830	Very strong	
2836	Medium	
2963	Very weak	
3165	Weak	
3962	Medium	ν_1 (H_2 stretch)

Q branch with relatively broad, intense, unresolved P and R branches (band FWHM 50 cm^{-1}). In contrast, all of the stronger, lower energy bands display structures more consistent with perpendicular transitions, i.e. they possess a prominent central band but lack broad P and R branch wings.

Apart from the band at 3962 cm^{-1} , which is almost unambiguously due to excitation of the H–H stretch vibration, we have found it difficult to determine secure vibrational assignments. The difficulties stem in part from the fact that the spectral data only extend down to 2500 cm^{-1} making it impossible to ascertain which (if any) of the bands represent fundamental transitions and which are due to combination or overtone transitions. Significantly, none of the bands possess the parallel structure expected for the ν_2 (N–H stretch) transition of the complex, implying that there has been a drastic decrease in the N–H stretch frequency from its free HN_2^+ value (3234 cm^{-1}). As there are no non-totally symmetric vibrations with frequencies over 1000 cm^{-1} (see Table 2) one is led to the conclusion that the 2500–3000 cm^{-1} bands must be due to overtones or combinations involving either the intramolecular HN_2^+ bending vibrations (ν_5 and ν_7), the intermolecular H_2 rock (ν_8) or quasi-degenerate intermolecular bends (ν_6 and ν_9). Possible

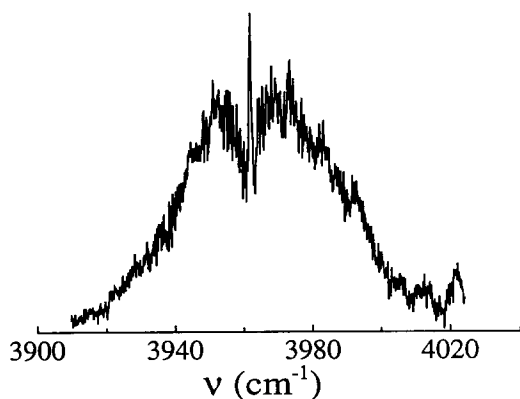


Fig. 5. Expanded view of the ν_1 band (H–H stretch) of $\text{H}_2\text{–HN}_2^+$. While the Q branch (at 3962 cm^{-1}) is clearly apparent, other rotational features are obscured because of lifetime broadening.

combinations are numerous, but the upper state probably involves the bending motions excited in combination with either the N–H or N–N stretch vibrations. Perpendicular bands predicted to fall in the same range include $\nu_2 + \nu_6$ and $\nu_2 + \nu_9$, $\nu_3 + \nu_5$, $\nu_3 + \nu_7$ and $\nu_3 + \nu_6$.

It should be emphasized that discussion of H_2HN_2^+ eigenvalues and eigenfunctions in terms of harmonic oscillator/rigid rotor wavefunctions is perhaps not entirely appropriate, especially for the floppy, low frequency intermolecular motions. Large-amplitude excursions [8], internal rotations [7], and tunnelling between equivalent nuclear configurations [26] have all been found to be significant in related proton-bound systems. The large rotational constant of H_2 (59.3 cm^{-1} [21]) implies that substantial potential barriers are required to quench effectively its internal rotation. Anharmonic interactions and couplings between the various low frequency motions should also be important. For instance, due to an increase in average intermolecular separation, exciting the intermolecular stretch (ν_4) should have the effect of markedly decreasing the frequencies for the quasi-degenerate low frequency bending motions (ν_6 and ν_9) and also the barrier to H_2 internal rotation.

5. Discussion

It is apparent from preceding experimental and theoretical work that the structures of proton-bound AHB^+ species are such that the proton is effectively shared by A and B, generally with each constituent being disposed with regard to the proton as they would be in the absence of the other. Thus, as HN_2^+ is linear and H_3^+ triangular, one would expect the $\text{H}_2\text{–HN}_2^+$ complex to be T-shaped, with the proton somewhat more strongly attached to N_2 . Such a structure would also be expected on the electrostatic grounds, a broadside approach of the HN_2^+ to the H_2 being favoured by charge–quadrupole forces. Generally the binding energy of the complex increases as the difference in the proton affinities decreases (and vice versa). When there is a large difference, the interaction is primarily an electrostatic one. However if the PAs are similar, the cohesion of the complex will derive from a bond having some chemical character, with the proton more or less equally shared between the constituents. The $\text{H}_2\text{–HN}_2^+$ complex lies between these extremes with a difference in the constituents' PAs of 18 kcal mol^{-1} and is characterized by a bond with a ΔH of $-7.2\text{ kcal mol}^{-1}$ (2520 cm^{-1}) [4,27].

The outcome of combining an H_2 molecule, a proton and ligands of varying proton affinities is nicely illustrated in a systematic ab initio study of the $\text{H}_2\text{–H}^+\text{–A}$ complexes [28] (A=He, Ne, Ar, Kr; PA $42.5\text{ kcal mol}^{-1}$, $48.1\text{ kcal mol}^{-1}$, $88.6\text{ kcal mol}^{-1}$ and $101.6\text{ kcal mol}^{-1}$ respectively). Unfortunately the $\text{H}_2\text{–H}^+\text{–Xe}$ complex, which, due to the similar proton affinities of N_2 and Xe (118.2 and $118.6\text{ kcal mol}^{-1}$ [3]), should have comparable properties to $\text{H}_2\text{–HN}_2^+$, was not included in the study. Nevertheless, the trends are clear. As the size (and concomitantly the proton affinity) of the rare gas increases, the system is transformed from one resembling an H_3^+ molecule perturbed by a rare gas atom loosely attached to one apex (e.g. He–H_3^+ , Ne–H_3^+), to

one consisting of an H₂ molecule bound in a T-shaped fashion to a protonated rare gas diatomic [28]. This latter situation should best approximate H₂–HN₂⁺.

Experimentally, for the H₂–HN₂⁺ system, the most striking results are the rather large complexation-induced red shifts for the N–H stretching vibration (> 700 cm⁻¹) and H₂ stretch (199 cm⁻¹). These two effects can be explained as follows. As the H₂ molecule makes a broadside approach to the proton end of the HN₂⁺ molecule, transfer of electron density from the H₂ σ bond to the protonated ion occurs, thereby weakening the H₂ bond (and leading to the formation of the incipient chemical bond). At the same time, the effective potential for the bridging proton becomes broader and flatter due to the presence of a second centre of attraction. Both effects are predicted by the ab initio computations with good agreement between the scaled H₂ stretch frequency (4011 cm⁻¹) and the experimental value (3962 cm⁻¹). For the N–H stretch (ν₂) it appears that the scaled ab initio result of 2538 cm⁻¹ is too high. However, for a very flat effective proton potential, the effects of anharmonicity may be extreme, and might not be properly taken into account by the scaling procedure. Significantly, extraordinarily large shifts for the characteristic proton stretch motion have also been noted for ArH⁺ [29] and ArHAr⁺ [30], where the frequency drops from 2588 cm⁻¹ in the diatomic to 1208 cm⁻¹ in the triatomic.

While extraction of detailed structural information from the IR spectra is frustrated by lifetime broadening which washes out almost all rotational structure, we noted in a parallel study of H₂–HCO⁺, where full rotational resolution of the H₂ stretch band was achieved, that the experimentally determined molecular parameters (intermolecular distance, intermolecular stretching frequency) were predicted rather well by the accompanying QCISD(T) ab initio calculations [8]. The

calculations predict a significantly shorter, stiffer intermolecular bond for H₂–HN₂⁺ compared to H₂–HCO⁺ (*r*_{int} 1.435 Å versus 1.744 Å, and ω_{int} of 438 cm⁻¹ compared to 320 cm⁻¹).

The almost complete absence of discernible rotational features in the H₂–HN₂⁺ spectrum in the 2500–4200 cm⁻¹ range implies extremely rapid vibrational energy redistribution. Contour simulations for the ν₁ band (H–H stretch), where at least a central Q branch is apparent (Fig. 5), suggest that rotational linewidths are of the order of 1–2 cm⁻¹, implying that redistribution occurs on picosecond time scales. A lack of resolved rotational features in the 2500–3000 cm⁻¹ range is evidence for similar rates for these lower vibrational levels.

Formerly it has been suggested that the red shift in the H–H stretch vibration accompanying complexation can be directly correlated with increases in both the strength of the intermolecular bond and rate of vibrational predissociation [8]. Such a connection presumably comes about because transfer of electron density from the H₂ σ bond to the protonated ion, which serves to establish the incipient intermolecular chemical bond and therefore to couple the H–H stretching motion with the intermolecular motion, also weakens the H₂ bond, resulting in the red shift. Though the available data are sparse, it seems to be the case that systems with large red shifts (e.g. H₃⁺, shift 251 cm⁻¹ [5] and H₂–HN₂⁺, shift 199 cm⁻¹) undergo rapid predissociation and consequently have blurred, featureless H₂ stretch bands, whereas systems associated with more modest red shifts (e.g. H₂–HCO⁺, shift 100 cm⁻¹ [8] and H₂–H₃O⁺, shift 115 cm⁻¹ [6]) survive long enough for rotational structure to be apparent.

6. Conclusions

In the present work we have sought to characterize the H₂–HN₂⁺ complex through

the application of *ab initio* theory and spectroscopy. This and related studies highlight the importance of the constituents' relative proton affinities in deciding the attributes (vibrational band shifts, predissociation lifetimes, dissociation energies) of the proton bound complex. Given the modest difference in H_2 and N_2 proton affinities (about 18 kcal mol^{-1}), one expects quite a degree of proton delocalization between the two moieties and a relatively strong intermolecular bond. These expectations are confirmed both in the substantial vibrational band shifts (-170 cm^{-1} for the H_2 stretch; more than 700 cm^{-1} for the N-H stretch) and rapid vibrational predissociation rates for both the H-H and N-H stretches. In $\text{H}_2\text{-HCO}^+$ where the difference in PAs is somewhat larger, vibrational band shifts are smaller and vibrational predissociation rates are considerably lower (10^{10} s^{-1}).

Unfortunately, due to extremely rapid vibrational energy redistribution and consequent line broadening, it is difficult to extract detailed structural information from the spectra which can be compared with the *ab initio* data. However, the computed and observed vibrational band shifts do agree well, engendering faith in the *ab initio* results. In order to learn more about the structure of the $\text{H}_2\text{-HN}_2^+$ complex and to establish the frequencies of the vibrational fundamentals it would be most useful to observe vibrational bands below 2500 cm^{-1} .

Acknowledgements

E.J.B. acknowledges the hospitality of Dr. G.T. Fraser and Dr. W.J. Lafferty at NIST Gaithersburg while the spectral data were being analysed. Support for this work under the Human Capital and Mobility Scheme "Structure and reactivity of Molecular Ions" BBW grant Nr. 93.02060 is acknowledged. This work is part of project No. 20-36153.92

of Schweizerischer Nationalfonds zur Förderung der wissenschaftlichen Forschung.

References

- [1] D. Adams and D. Smith, *Int. J. Mass Spectrom. Ion Phys.*, 21 (1976) 349.
- [2] D. Adams and D. Smith, *J. Phys. B*, 9 (1976) 1439.
- [3] S.G. Lias, J.E. Bartmess, J.F. Liebman, J.L. Holmes, R.D. Levin and W.G. Mallard, *J. Phys. Chem. Ref. Data*, 17 (1988).
- [4] K. Hiraoka, P.P.S. Saluja and P. Kebarle, *Can. J. Chem.*, 57 (1979) 2159.
- [5] M. Okumura, L.I. Yeh and Y.T. Lee, *J. Chem. Phys.*, 88 (1988) 79.
- [6] M. Okumura, L.I. Yeh, J.D. Myers and Y.T. Lee, *J. Phys. Chem.*, 94 (1990) 3146.
- [7] J.M. Price, M.W. Crofton and Y.T. Lee, *J. Chem. Phys.*, 91 (1989) 2749.
- [8] E.J. Bieske, S.A. Nizkorodov, F.R. Bennett and J.P. Maier, *J. Chem. Phys.*, 102 (1995) 5152.
- [9] S.A. Nizkorodov, J.P. Maier and E.J. Bieske, *J. Chem. Phys.*, 102 (1995) 5570.
- [10] E.J. Bieske, *J. Chem. Soc., Faraday Trans.*, 91 (1995) 1.
- [11] E.J. Bieske, A.M. Soliva, A. Friedmann and J.P. Maier, *J. Chem. Phys.*, 96 (1992) 4035.
- [12] E.J. Bieske, A.M. Soliva and J.P. Maier, *J. Chem. Phys.*, 94 (1991) 4749.
- [13] C.J.F. Boettcher and P. Borderwijk, *Theory of Electric Polarization*, Elsevier, Amsterdam, 1978.
- [14] L.M. Wolniewicz, *J. Chem. Phys.*, 45 (1966) 515.
- [15] W.P. Kraemer, A. Kormornicki and D.A. Dixon, *Chem. Phys. Lett.*, 105 (1986) 87.
- [16] J.A. Pople, M. Head-Gordon and J. Raghavachari, *J. Chem. Phys.*, 90 (1989) 4635.
- [17] R. Krishnan, J.S. Binkley, R. Seeger and J.A. Pople, *J. Chem. Phys.*, 72 (1980) 650.
- [18] M.J. Frisch, G.W. Trucks, J.B. Foresman, M.A. Robb, M. Head-Gordon, E.S. Replogle, R. Gomperts, J.L. Andres, K. Raghavachari, J.S. Binkley, C. Gonzalez, R.L. Martin, D.J. Fox, D.J. DeFrees, J. Baker, J.J.P. Stewart and J.A. Pople, *GAUSSIAN 92/DFT, Revision G.2*, Gaussian, Inc., Pittsburgh, PA, 1993.
- [19] R.J. Saykally, T.A. Dixon, T.G. Anderson, P.G. Szanto and R.C. Woods, *Astrophys. J. Lett.*, 205 (1976) 101.
- [20] Y. Kabbadj, T.R. Huet, B.D. Rehfluss, C.M. Gabrys and T. Oka, *J. Mol. Spectrosc.*, 163 (1994) 180.
- [21] K.P. Huber and G. Herzberg, *Molecular Spectra and Molecular Structure IV. Constants of Diatomic Molecules*, van Nostrand Reinhold, New York, 1979.
- [22] K. Hirao and S. Yamabe, *Chem. Phys. Lett.*, 79 (1981) 279.
- [23] R.S. Grev, C.L. Janssen and H.F. Schaefer III, *J. Chem. Phys.*, 95 (1991) 5128.
- [24] W.J. Hehre, L. Radom, P.v.R. Schleyer and J.A. Pople,

- Ab Initio Molecular Orbital Theory, Wiley, New York, 1986.
- [25] R.J. Le Roy, University of Waterloo Chemical Physics Report CP-330, LEVEL 5.0, 1991.
- [26] M. Bogey, H. Bolvin, C. Demuynck and J.L. Destombes, Phys. Rev. Lett., 58 (1987) 988.
- [27] R.G. Keesee and A.W. Castleman, Jr., J. Phys. Chem. Ref. Data, 15 (1986) 1011.
- [28] P. Hobza and R. Zahradnik, Chem. Phys. Lett., 208 (1993) 497.
- [29] J.W.C. Johns, J. Mol. Spectrosc., 106 (1984) 124.
- [30] J. Nieminen and E. Kauppi, Chem. Phys. Lett., 217 (1994) 31.